Journal of Harbin Engineering University
ISSN: 1006-7043

Vol 47 No. 7
July 2026

Biological and Optical Applications of $Y_2Ti_2O_7$ Nanoparticle Using Microwave – Assisted Method

S. Devi[1*], E. Kavitha[2], C. Andal[3], D. Preethi[4]

[1*]Research Scholar, Department of Physics, Dr. M. G. R. Educational and Research Institute, Chennai-600095, Tamil Nadu, India.

[2]Professor, Department of Physics, Dr. M. G. R. Educational and Research Institute, Chennai-600095, Tamil Nadu, India.

[3]Professor, Department of Physics, Dr. M. G. R. Educational and Research Institute, Chennai-600095, Tamil Nadu, India.

[4]Research Scholar, Department of Physics, Dr. M. G. R Educational and Research Institute, Chennai-600095, Tamil Nadu, India.

Abstract

The Pyrochlore type Yttrium Titanate ($Y_2Ti_2O_7$) nanoparticle (YTO) was successfully synthesized by microwave assisted method with the suitable temperature conditions. To analyze, several properties of physical, chemical, optical and biological nature, the synthesized $Y_2Ti_2O_7$ (YTO) nanoparticle was employed to such studies including XRD, SEM, EDAX, FTIR, UV-vis-NIR, PL, TG/DTA and anti-microbial activities. The XRD results confirmed the lack of secondary phases associated with the Y - Ti - O complex structure. In the morphological result shows the uniform semi-cylindrical domains were eventually identified and distributed with the presence of Yttrium and Titanium oxides which suggesting the formation of $Y_2Ti_2O_7$ (YTO) nanoparticles using SEM and EDAX analysis. Also, FTIR shows the Y – O stretching vibration and Ti^{4+} complex, in the synthesized $Y_2Ti_2O_7$ (YTO) nanoparticle. For its potential optical applications, the optical studies were carried out from PL spectrum and UV-vis-NIR with Tauc plot analyses of straight energy transition in the range of band gap (3.2 eV). Moreover, TG/DTA was used to analyze the thermal nature of the nanoparticle, for the determination of its thermal stability. In addition, EDAX examination revealed that the synthesized $Y_2Ti_2O_7$ (YTO) nanoparticle includes solely Y, Ti and O with no impurities. The biological application of $Y_2Ti_2O_7$ (YTO) nanoparticle was confirmed with anti-bacterial and anti-fungal activities including the zone of inhibition of organisms was dose dependently increased.

Keyword: PXRD, SEM, EDAX, FTIR, UV, PL, TG/DTA, Anti-microbial activity.

1. Introduction

In recent years, rare earth elements gained significant interest due to their distinctive potential applications across various domains [1-4]. In these elements, Pyrochlore - structured nanomaterial $Y_2Ti_2O_7$ (YTO) nanoparticle is recognized for their stability as complex oxides under rigorous conditions of irradiation, excessive temperatures and high pressure [5, 6]. These types of nanomaterials possess magnetic, catalytic, high melting points, less thermal conductivity and exhibit outstanding chemical stability and mechanical stability [7, 8]. $Y_2Ti_2O_7$ (YTO) nanoparticle is prominent material for its effectiveness as a superior ionic conductor and exhibits exceptional microwave dielectric attributes [9, 10]. It is an insulator material with band gap energy of about 3.2 eV, characterized by electronic density of states emerging from the combination of O-2p states along with Ti-3d and Y-4d states in $Y_2Ti_2O_7$ (YTO) nanoparticle [11]. $Y_2Ti_2O_7$ (YTO) nanoparticle can be synthesized through various routes such as sol gel method, pechini approach, co-precipiation and solvothermal method [12-14]. Among these methods, the microwave – assisted precipitation route provides several benefits such as rapid, consistent heating with negligible loss of energy and production of

high-purity materials with reduced structural flaws [15]. Microwaves can permeate into the nanomaterials and engage directly with the internal atoms to produce heat, in contrast to traditional conventional heating which occurs from the exterior to the interior [16].

Several researchers have attempted with $Y_2Ti_2O_7$ (YTO) nanoparticle as dopants, nanocomposites for various photocatalytic, Oxide Dispersion Strengthened (ODS) steels and photovoltaics applications such as Zhang et al. have reported Si-doped with $Y_2Ti_2O_7$ (YTO) nanoparticle ceramics through sol-gel method with electromagnetic wave absorption application [17]. The $Y_2Ti_2O_7$ (YTO) nanoparticle ceramic is regarded as a potential microwave – absorbing material based on its pyrochlore structure and superior chemical stability; however, its practical application has been constrained by low intrinsic dielectric loss and a narrow absorption bandwidth [18]. This study proposed the photochemical synthesis of $Y_2Ti_2O_7$ (YTO) nanoparticle for the photocatalytic chemical degradation of brilliant green (BG) and the disinfection of Escherichia coli (E. coli) [19].

Owing to the above nature in the work we have chosen $Y_2Ti_2O_7$ (YTO) nanoparticle to analyze for both luminescence and biomedical applications. There is a significant biomedical application in anti-bacterial and anti-fungal action of synthesized nanoparticles against bacteria such as Staphylococcus species and E.coli were carried out. Anti-bacterial activity is applied to treat the bacterial infections by killing or inhibiting the growth of bacterial and prevents infection on medical devices and wound dressings.

In the current research work, the $Y_2Ti_2O_7$ (YTO) nanoparticles are synthesized by the microwave - assisted precipitation process. The structural, morphological, elemental, optical and the thermal properties of $Y_2Ti_2O_7$ (YTO) nanoparticle are examined using powder XRD, SEM, EDAX, FTIR, UV-vis-NIR, PL and TG/DTA analyses were reported. Furthermore, the anti-microbial applications of $Y_2Ti_2O_7$ (YTO) nanoparticle are primarily investigated using anti-microbial activities which are extensively utilized in bio-medical fields.

2. Materials And Methods

2.1 Synthesis of $Y_2Ti_2O_7$ nanoparticle using Microwave Assisted method

The chemicals, such as Yttrium Nitrate hexahydrate [$Y(NO_3)_3.\ _6H_2O$ 99.9% pure], Titanium Chloride [$TiCl_4$] and sodium hydroxide pellets [NaOH 98% pure], were procured from SRL (India) and utilized without any treatment and purification.

A translucent solution was created by Yttrium Nitrate Hexahydrate [$Y(NO_3)_3.\ _6H_2O$] (3.83 g) and Titanium Chloride [$TiCl_4$] (1.89 g) in 100 ml solution of distilled water and are stirred constantly with equal molar ratio. After obtaining clear solution, sodium hydroxide pellets [NaOH] (2.8 g) were added. A white precipitate formed after an hour of intense stirring. NaOH was then used to neutralize the resultant white precipitate solution to pH 12. For fifteen minutes, the resulting solution was heated with power (700 W) in a microwave. The precipitate was completely dried and washed with distilled water which was then filtered in Whatmann filter paper . A muffle furnace was used for the additional annealing step, which lasted two hours at 850 °C. The obtained nanoparticles was collected for characterisation analyses after being finely ground in a mortar as shown in Fig.1.

Fig. 1 Image of Yttrium Titanate ($Y_2Ti_2O_7$) nanoparticle

3. Results And Discussions

3.1 Powder X-Ray Diffraction (PXRD) Analysis

In nanotechnology, Powder X-ray Diffraction (PXRD) is a non-invasive and effective technique employed to analyse nanomaterials with diameters from 1 to 100 nm. X-ray wavelengths perform at

the atomic scale, facilitating XRD to efficiently elucidate structural features including phase composition, crystallite size and lattice strain. Powder X-ray diffraction has been extensively used for the identification of sample components through search/match analysis from JCPDS [20]. The structural quality of the synthesized $Y_2Ti_2O_7$ (YTO) nanoparticle using microwave - assisted method was obtained from the PXRD instrument X'pert PRO – PANalytical of Cu Kα radiation, covering spectral region of 10 ° to 80 °at a rate of 5°/min. From the results mentioned in the Fig. 2 indicated that, a good match between the diffraction patterns obtained from JCPDS no. 89-2065 was found. The strong diffraction peaks of 2θ values observed was 29.12°, 30.60°, 50.96° and 60.88° corresponds to the hkl values of (3 1 1), (2 2 2), (4 4 0) and (6 2 2). The phase purity of the formed nanoparticle was confirmed by the lack of secondary phases associated with the Y-Ti-O complex structure. In this diffraction pattern exhibits the pyrochlore - oxide structure of FCC (Face Centered Cubic) lattice parameter in the space group of Fd3m was relevant with the reported [21]. Furthermore, it was known that when the cation antisite disorder rises, the pyrochlore structure transforms into a defect fluorite structure by order-disorder transformation. No other impure particle phases of Y_2O_3 and TiO_2 were deducted which confirms the pure nature of $Y_2Ti_2O_7$ (YTO) nanoparticles. Additionally, the ratio of intensity of the (3 3 1) and (4 0 0) reflections can be used to quantify the standard of cation antisite disorder.

The predicted point of 0.71 for a structure of pyrochlore was reported, which was [22] extremely near to the estimated I_{331}/I_{400} ratio of approximately 0.79 for the $Y_2Ti_2O_7$ (YTO) nanoparticle in our study.

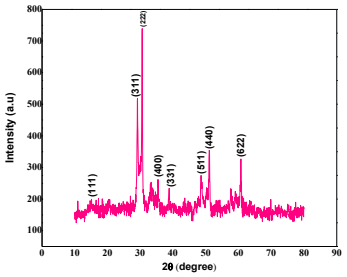

Fig. 2 Powder X-ray diffraction pattern of Yttrium Titanate ($Y_2Ti_2O_7$) nanoparticle

3.2 Morphological Analyses

3.2.1 Scanning Electron Microscope (SEM) analysis

Scanning Electron Microscopy (SEM) is considered as a versatile technology for the analysis of nano and micro-structures, with diverse area of applications. This technique demonstrates findings about the topograph and composition of the surfaces. It captures data obtained from signals generated by certain interactions with the material compositions. SEM conveys knowledge about the characteristics property like surface topograph, composition, morphology and information about the crystallographic nature [23]. In this study, SEM was used to perform morphological analysis in order to further examine the impact of Yttrium Titanate $Y_2Ti_2O_7$ (YTO) nanoparticle Fig. 3. The instrument Carel Zeiss, model Evo 18 was employed to carry out the microscopic characterisation. The results indicated that, the produced Yttrium Titanate $Y_2Ti_2O_7$ (YTO) nanoparticle showed annular shape with the good quality and nanosize of 99.32 nm. Fig. 3 shows the SEM image of the synthesized $Y_2Ti_2O_7$ (YTO) nanoparticle with rod like structure in few nanoparticles. Most of the $Y_2Ti_2O_7$ (YTO) nanoparticles shows a uniform semi-cylindrical domains which was due to the cluster of its 99.32 nm size. Also, as it is seen in the Fig. 3 the majority of pyrochlore particles has dimensions between 99.32 nm to 128.4 nm in a slight elongation. The average particle size surface area was calculated and it is 108.67 nm. Thus, from the obtained result the particle size and morphology was eventually distributed and well suited with the earlier

reported [24].

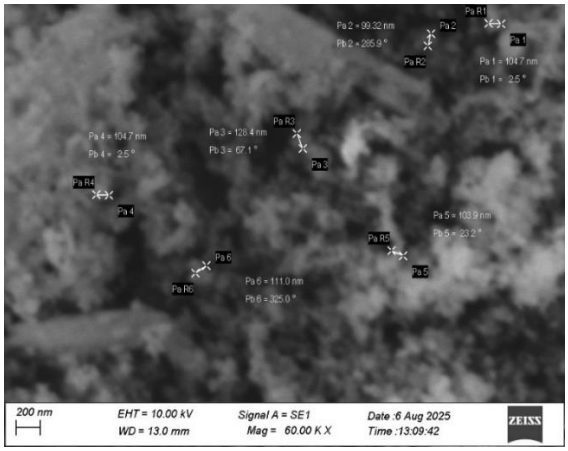

Fig. 3 SEM analysis of Yttrium Titanate ($Y_2Ti_2O_7$) nanoparticle

3.2.2 Energy – Dispersive X-ray Analysis (EDAX)

Energy Dispersive X-ray (EDAX) analysis is an elemental interpretation approach linked to electron microscopy that generates distinctive X-rays, indicating the presence of elements in the specimens. The EDAX technique is valuable in pharmacological research, particularly in drug delivery studies, where it serves as a crucial instrument for detecting nanoparticles. EDAX is utilised in the examination of environmental pollution and in the characterisation of minerals bio accumulated in tissues [25]. Oxford instrument is used to perform the EDAX analysis. Presence of different element in the Yttrium Titanate nanoparticle was evaluated by EDAX analysis. The result findings demonstrated that the synthesized nanoparticle's surface contains only Y, Ti, and O, without any impurities and the atomic ratio of Y: Ti: O was 18.51: 0.76: 80.72 Fig. 4. This result confirms that the $Y_2Ti_2O_7$ (YTO) nanoparticle's stoichiometric ratio is 2:2:7 and this was correlated with the reported [26].

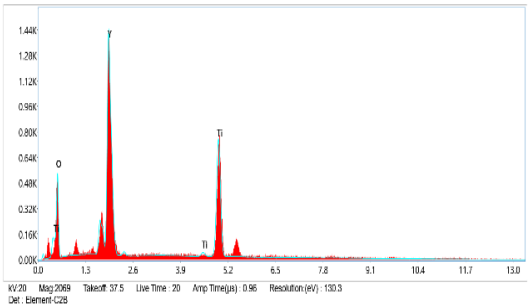

Fig. 4 EDAX analysis of Yttrium Titanate ($Y_2Ti_2O_7$) nanoparticle

3.2.3 Fourier Transform Infrared spectroscopy (FTIR) analysis

FTIR spectra was used to track the structural alterations of compounds throughout the preparatory process in order to examine the reaction and uniform distribution mechanism of reactants. The $Y_2Ti_2O_7$ (YTO) nanoparticle was characterised using Fourier Transform Infrared Spectroscopy (FTIR, Perkin Elmer, Spectrum 2 Instrument) in a spectral region of 4000 – 400 cm^{-1}, with a scan speed of 20 nm/min. Fig. 5, shows the findings at 3356.8 cm^{-1} and 1622.2 cm^{-1} are due to the hydroxyl group and OH stretching vibration, which can be explained by the moisture in the samples [27].

The Fourier Transform Infrared (FTIR) spectrum of the synthesized material show different vibrational characteristics correlated with metal-oxygen frameworks and residual nitrate species. The prominent absorption bands detected at 1385-1398 cm^{-1} are associated to asymmetric stretching of N-O bands in the nitrate (NO_3^-) ions, obtained from the yttrium nitrate hexahydrate precursor. The band at around 1204 cm^{-1} corresponds to the symmetric stretching mode of nitrate ions. These assignments align with the literature, indicating that nitrate ions generally have significant IR absorption in the 1300-1500 cm^{-1}range [28, 29]. The small band at around 2922 cm^{-1}, correlated for asymmetric C-H stretching of aliphatic $–CH_2$ groups. Similar bands have been extensively reported in TiO_2 and mixed-oxide systems, typically ascribed to trace organic chemicals or hydrocarbons adsorbed from the environment, or residual solvents employed during synthesis. The $Y_2Ti_2O_7$ (YTO) nanoparticle pyrochlore structure is solely inorganic; thus, the appearance of this band is extrinsic and does not indicate any structural integration of carbon-containing molecules.

This suggests that there was a strong coordination interaction between Ti^{4+} and Y^{3+} with the band vibration at 560 cm^{-1} and 460 cm^{-1} for the formation of TiO and YO to conform the presence of $Y_2Ti_2O_7$ (YTO) nanoparticle [30, 31]. From the above observed results clearly indicate that there was no other additional peaks were found during the formation of the desired nanoparticles of $Y_2Ti_2O_7$ (YTO) nanoparticle. This infrared spectral

studies, proves that many functional groups wavelength signal from the synthesized nanoparticle has appeared.

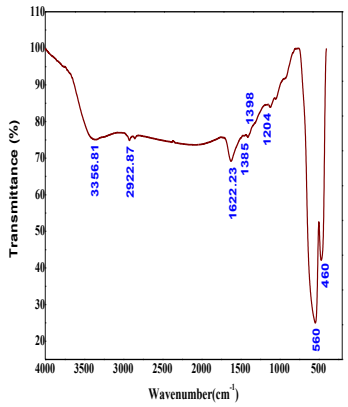

Fig. 5 FTIR analysis of Yttrium Titanate ($Y_2Ti_2O_7$) nanoparticle

3.3 Optical Studies

3.3.1 UV-Vis-NIR Analysis

UV-Vis-NIR spectroscopy study was employed to find the changes in electronic energy levels within the molecules arising due to transfer of e^{-s} from the Valence band (V_B) to Conduction band (C_B). Since $Y_2Ti_2O_7$ (YTO) nanoparticle has high refractive index than the transparent ceramics [32]. It has been observed that the optical property which includes absorption and transmission features were determined using UV-vis-NIR spectroscopy within 200 – 1200 nm range (Perkin – Elmer Lambda 35 spectrophotometer, 100 nm/min^{-1} scan speed, 1 nm spectral bandwidth). The UV-vis-NIR absorbance and transmittance spectra of Yttrium Titanate nanoparticle was analysed and the results represented in the Fig. 6 and 7.

The absorbance was obtained between 200 nm to 1200 nm of wavelength. It shows that the broad wide peak at λ = 384.7 nm in the visible light region. Since, this material was a good ionic conductor [33], the electrons move from the 2p states of O molecule (which forms top of V_B) to 3d states of Ti molecule (which forms bottom of C_B). Overall, at 250 nm – 315 nm region, shows the strong absorbance state. The results clearly indicated that, the absorbance of the Yttrium Titanate was higher at (384.7 nm) and the absorbance was started to decrease in the visible region. It was due the trivalent and tetravalent cations of Y^{3+} and Ti^{4+} of the $Y_2Ti_2O_7$ (YTO) nanoparticle was coordinated with eight and six oxygen ions.

In addition to affirm the acceptable quality of $Y_2Ti_2O_7$ (YTO) nanoparticle, the UV-vis-NIR Transmittance spectra of the $Y_2Ti_2O_7$ (YTO) nanoparticle was shown in Fig. 7 which explains the significant decrease in transmittance at λ = 384.7 nm, the substance absorbs the greatest energy in that specific wavelength range. This wavelength falls inside the near-UV range, at the boundary of the visible spectrum.

It shows that the UV-vis-NIR transmittance spectra of $Y_2Ti_2O_7$ (YTO) nanoparticle was analysed from 200 nm – 1200 nm. From the graph, the wavelength of 200 nm to 400 nm region, as the wavelength increased the transmittance also increased in the visible and NIR region. Here, the transmittance was above 55%, since the refractive index varies with wavelength for most of the transparent materials [34]. Besides the increased transparency results in stronger emission, which consequently reduces the re-absorption of emitted light. This nature was more advantageous for the development of opto-electronic devices [35].

By using the absorbance and the transmittance spectrum, the bandgap was also calculated and also The Tauc [36] relation is used to compute the optical band gap energy. The equation is,

$$(\alpha h\nu)^{1/n} = A\,(h\nu - E_g) \quad \text{---------- (1)}$$

Here, hν is the photon energy, α is the absorption coefficient and E_g is the optical band gap, A is a proportionality constant, and n is Tauc exponent, which depends on the type of material about its band gap energy:

n = ½ for a direct band gap and n = 2 for indirect band gap. The graph Fig. 8 was plotted against (αhν) versus energy and the obtained band gap was 3.2 eV was consistent with the earlier reported [37]. This optical band gap graph confirms the semiconducting nature of the $Y_2Ti_2O_7$ (YTO) nanoparticle and the wide bandgap facilitates the UV and visible light emission which was applicable

for photo-electronic devices [38]. The obtained UV-vis-NIR results revealed that the material can be used for various OLED applications such as sensors, fluorescence and catalytic activities [39,40].

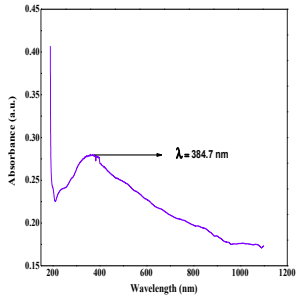

Fig. 6
UV-vis-NIR Absorbance spectra analysis of Yttrium Titanate ($Y_2Ti_2O_7$) nanoparticle

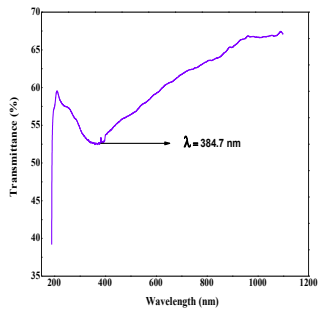

Fig. 7
UV-vis-NIR Transmittance spectra analysis of Yttrium Titanate ($Y_2Ti_2O_7$) nanoparticle

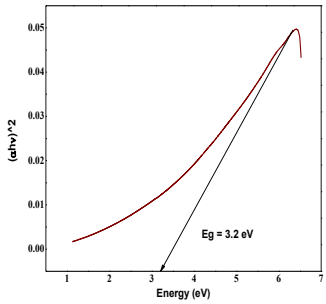

Fig. 8 Tauc plot analysis of Yttrium Titanate ($Y_2Ti_2O_7$) nanoparticle

3.3.2 Photoluminescence (PL)

PL is a process where a material observes photons in light energy causing electrons to jump to higher energy states, which is excitation level and then emits light as those electrons return to lower energy state which is relaxation level. It is a non-destructive method used to analyse the structural and the optical properties of compounds. The instrument used for characterization of the synthesized $Y_2Ti_2O_7$ (YTO) nanoparticle was Perkin Elmer, model LS 45, with 200 nm to 900 nm. The PL spectrum of $Y_2Ti_2O_7$ (YTO) nanoparticle was performed to find the optical properties at room temperature. The Fig. 9 shows obtained PL spectrum of $Y_2Ti_2O_7$ (YTO) nanoparticle.

From the graph, it shows the particle excited at 360 nm displays a sharp narrow emission band meant to trigger electronic transitions and luminescence in the nanomaterial, followed by a small hump at 372 nm. This hump caused below the conduction band of $Y_2Ti_2O_7$ (YTO) nanoparticle in the near band edge emission signifying the good quality with less structural defects. This band edge emission was ascribed to the conjugation of excitons [41]. The subsequent three prominent peak emission of PL at a wavelength of 406 nm, 443 nm and 490 nm was well suited within the bluish green region. In the relaxed emission state, the first 406 nm emission peak was attributed to the charge transfer within the tetravalent ions. Also, in accordance with the red emission spectral region shows a small narrow peak at 722 nm and a small peak at 752 nm. These PL spectra confirm that the materials nature was suitable for OLED applications. Moreover, the several emission peaks of the luminescence pathway leads to beneficial for Photocatalytic process and Bio-Imaging applications [42].

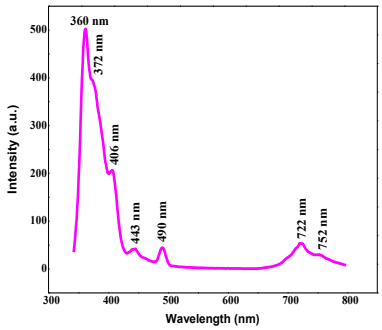

Fig. 9 Photoluminescence spectrum of Yttrium Titanate ($Y_2Ti_2O_7$) nanoparticle

3.4 Thermogravimetric and Differential Thermal Analyses (TG/DTA)

TG/DTA (Thermogravimetry / Differential Thermal Analysis) evaluates mass variations (TG) and thermal phenomena (DTA) of a sample during heating. It identifies decomposition, oxidation and phase transitions by determining whether a weight loss or weight gain is endothermic or exothermic, therefore revealing essential information involving thermal stability, composition and reaction kinetics. The thermal stability of synthesized material was been analysed by the use of TGA, SII Nanotechnology Inc., Japan, EXSTAR6200 TG/DTA and Perkin Elmer, TGA 4000. In the Thermal Gravimetric - Differential Thermal Analysis (TG-DTA) of Yttrium Titanate ($Y_2Ti_2O_7$) (YTO) nanoparticle, the weight changes of the sample as the temperature changes are examined. The TG curve indicates a steady decrease in weight up to roughly 550°C; this weight loss was brought on by the organics dehydration and decomposition. It demonstrates, how the weight loss indicated by the TG curve decreased steadily as the temperature increased. This was explained by removal of absorption of water [43], the ethanol reminders being evaporated and eliminated from the heated granules. In TGA curve, there are three distinct weight losses stages can be observed at 101°C, 401°C and 680°C. The first stage at 101°C was due to volatilization, decomposition of not only water but also ethanol. In the next stage 401°C occurs, because of organic substances burning and evaporation. The final stage of the material shows excellent thermal stability and it can be applied to high temperature applications of pyrochlores. From the graph, an arrow point at TG curve 550°C denotes a sharp weight change occurred due to the disordered pyrochlore which was attributed by the variation in temperature, composition and pressure [44].

In DTA, it reveals the presence of minor endothermic peak between 55°C to 60°C is an indicative of the evaporation of absorbed water molecules in the synthesis process. Also, it shows 200°C to 400°C pinned on the complex of citric acid combustion [7]. Additionally, the pyrochlore oxide phase development was by means of the broad and strong exothermic peak at 600.41°C Fig. 10. From the above TG/DTA results, it may be concluded that $Y_2Ti_2O_7$ (YTO) nanoparticle exhibits excellent thermal stability and well agreed with the previously reported [26]. This TG/DTA results reveals that the material may be used for applications below its melting point.

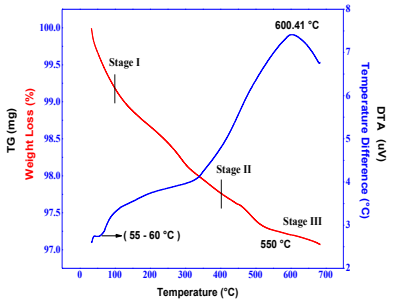

Fig. 10 TG–DTA curve of Yttrium Titanate ($Y_2Ti_2O_7$) nanoparticle

3.5 Biological Evaluation

3.5.1 Anti-bacterial activity

Anti-microbial activity represents the capacity of a chemical substance such as an antibiotic, antiseptic or natural extract – to eliminate bacterial or impede their development and reproduction. It defends against bacteria, viruses and fungus to prevent infections or avoid contamination. Every chemical compound has a different way of working against germs. No chemical molecule has a completely understood antibacterial mechanism. The enhanced release of

antibacterial metal ions from chemical compound surfaces is linked to some mechanisms, while others are related to the physical structure of the chemical compound. The anti-bacterial activity of $Y_2Ti_2O_7$ (YTO) nanoparticle was evaluated using well diffusion method against Gram-positive and Gram-negative bacteria, including S. aureus and E. coli. The anti-bacterial efficacy of $Y_2Ti_2O_7$ (YTO) nanoparticle was determined by evaluating the zone of inhibition at various concentrations (10 µg, 20 µg, and 30 µg) against S. aureus and E. coli in Fig. 11. The results demonstrate that $Y_2Ti_2O_7$ (YTO) nanoparticle displays superior inhibitory effects against Gram-positive bacteria, with a zone of inhibition of 18 mm, and against Gram-negative bacteria, with a zone of inhibition of 19 mm, at an optimum concentration of 30 µg, illustrated in Table. 1. The bacteria were cultured overnight in nutritious broth at 37 °C in a rotating shaker and subsequently centrifuged for approximately 5 mins at the 10,000 rpm. The pellet is fully dissolved in the double - distilled water and resultant cell density had been standardized spectrophotometrically at A610 nm. Various concentrations of samples were generated by recombining them with a methanol solution. The test microorganisms were injected into the appropriate medium utilizing the spread plate technique with 10 µl (10 cells/ml) derived from 24 - hr bacterial cultures in nutrient broth. Upon solidification of medium, filter paper wells of 5 mm in diameter, infused with extracts, were placed onto the implanted plates. Amoxicillin (10 µg) utilized as a reference

for anti-bacterial evaluation. The plates

were consequently incubated at 37 °C for almost 24 hrs [45]. Following the analysis of the plates, the width of growth inhibition zone surrounding the sample disc has been measured. The dimensions of inhibitory zones were measured in mm. The results revealed that, the zone of inhibition of Yttrium Titanate $Y_2Ti_2O_7$ (YTO) nanoparticle was dose dependently increased. Different concentration. 10, 20 and 30 µg/mL of Yttrium Titanate $Y_2Ti_2O_7$ (YTO) nanoparticle treatment showed 5, 12 and 18mm of zone of inhibition against *Staphylococcus aureus* and 5, 13 and 19 mm of zone of inhibition against *E. coli* in Table. 1.

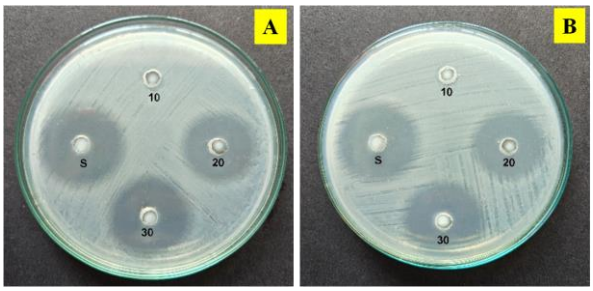

Fig. 11 Antibacterial activity of Yttrium Titanate ($Y_2Ti_2O_7$) nanoparticle against (A) Gram-positive (Staphylococcus aureus) and (B) Gram-negative (E. coli) bacterial strains.

3.5.2 Anti-fungal activity

The anti-fungal efficiency of $Y_2Ti_2O_7$ (YTO) nanoparticle was examined against fungal infections, including Candida albicans. The fungal inoculum retaining these pathogens was obtained from cultures aged 5 to 10 days, grown on the Potato Dextrose Agar substrate medium. A portion of about 8 - 10 mL distilled water had been introduced to those petri plates to collect conidia using a sterile spatula. The spore suspension was normalized to nearly 10^5 spores/ml using a spectrophotometer at A595 nm. Point inoculation was performed on potato dextrose agar substrates using 10-day-old fungal cells. Filter paper wells about 5 mm in diameter were injected with 100 µg of prepared $Y_2Ti_2O_7$ (YTO) nanoparticle and placed on plates inoculated with the test organisms. A positive control of ~10 µg of Standard (Fluconazole) is employed. The outcomes have been reported following incubation at 28°C for 72 hours [46]. The anti-microbial assays were carried out in triplicate, with the average functioning as

S. No	**Pathogenic Bacteria**	**Zone of Inhibition (mm)**			**Standard (Amoxicillin)**
		10 µg	**20 µg**	**30 µg**	
1.	*Staphylococcus aureus*	05	12	18	22
2.	*E. coli*	05	13	19	22

Table. 1 Zone of Inhibition of Yttrium Titanate ($Y_2Ti_2O_7$) nanoparticle against bacterial strains

the final measurement. Anti-fungal activity of

Yttrium Titanate nanoparticle was evaluated against *Candida albicans* and the results represented in the Fig. 12 explored that, 10, 20 and 30 µg/mL of Yttrium Titanate treatment $Y_2Ti_2O_7$ (YTO) nanoparticle showed 5, 9 and 14mm of inhibition and standard antifungal agent, Fluconazole showed 20mm in Table. 2. It was confirmed that the antifungal action was dose-dependent since the inhibitory response was proportionate to the applied concentration. The better coordination of yttrium titanate compound in the ligand framework is often responsible for the enhanced antifungal effect. Table. 3 reveals that $Y_2Ti_2O_7$ (YTO) nanoparticle exhibits antifungal efficacy against Candida albicans, with a notable zone of inhibition measuring 14 mm at an amount of 30 µg Fig. 12.

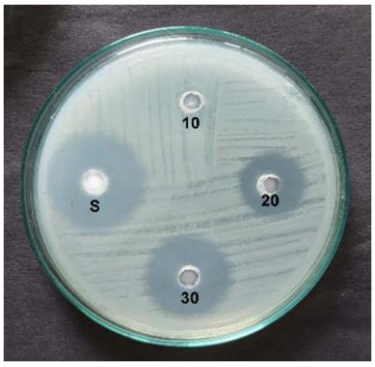

Fig. 12 Antifungal activity of Yttrium Titanate ($Y_2Ti_2O_7$) nanoparticle against Candida albicans

S.No	Pathogenic Fungi	Zone of Inhibition (mm)			Standard (Fluconazole)
		10 µg	20 µg	30 µg	
1.	*Candida albicans*	05	09	14	20

Table. 2 Zone of Inhibition of Yttrium Titanate ($Y_2Ti_2O_7$) nanoparticle against Candida albicans

4. Conclusion

In this research we have used time efficient and environmental friendly microwave-assisted approach to prepare Yttrium Titanate ($Y_2Ti_2O_7$) (YTO) nanoparticle. Various techniques were applied to analyze the nanoparticle properties and the pyrochlore oxide structure of FCC nature retained, which was confirmed by powder XRD. The uniform semi – cylindrical domain image with the size of 99.32 nm were confirmed by SEM analysis. FTIR spectrum affirms using the presence of hydroxyl group, Y – O', also Ti – O functional group. In addition to that, EDAX analysis proved the synthesized $Y_2Ti_2O_7$ (YTO) nanoparticle contains only the Yttrium (Y), Titanium (Ti) and Oxygen (O), without any impurities along with their correct stoichiometric composition 2:2:7 was successfully assessed. UV-vis-NIR spectrum confirmed that, the maximum absorbance was noted at the UV region whereas it's started to down in the visible region. Furthermore, in Tauc's plot, the result revealed that, the $Y_2Ti_2O_7$ (YTO) nanoparticle undergoes a direct energy transition along with a band gap of 3.2 eV. Moreover, the as prepared nanomaterial demonstrated good thermal stability even at elevated temperature which was confirmed by TG/DTA results. The obtained luminescence emission shows the charge transfer within the tetravalent ions. Also, the observed PL peaks reveals not only in the bluish green region but also in the red emission region. Yttrium Titanate nanoparticle shown possible antimicrobial measures against gram-positive and gram-negative bacterial strains as well as fungus strains for the potential application in biological field. Anti-fungal activity of compound was evaluated and the interaction with fungal cell membranes. The potential optical application of $Y_2Ti_2O_7$ (YTO) nanoparticle was confirmed with the PL studies and UV-vis-NIR results for various OLED device applications.

Reference

1 Wu YS, Liu XJ, Han DD, Song XY, Shi L, Song Y, Niu SW, Xie YF, Cai JY, Wu SY, Kang J, Zhou JB, Chen ZY, Zheng XS, Xiao XH, Wang GM. Electron density modulation of $NiCo_2S_4$ nanowires by nitrogen incorporation for highly

efficient hydrogen evolution catalysis. Nat. Commun. 2018; 9: 1425.

2 Ouyang D, Ye YQ, Wu CY, Xiao K, Liu ZQ. Heterostructures composed of N-doped carbon nanotubes encapsulating cobalt and beta-Mo_2C nanoparticles as bifunctional electrodes for water splitting. Angew. Chem. Int. Ed. 2019; 58: 4923-4928.

3 Wu NN, Xu DM, Wang Z, Wang FL, Liu JR, Liu W, Shao Q, Liu H, Gao Q, Guo ZH. Achieving superior electromagnetic wave absorbers through the novel metal–organic frameworks derived magnetic porous carbon nanorods. Carbon. 2019; 145: 433 – 444.

4 Zhang WY, Liang SQ, Fang GZ, Yang YQ, Zhou J. Ultra-high mass-loading cathode for aqueous zinc-ion battery based on graphene-wrapped aluminium vanadate nanobelts. Nano-Micro Lett. 2019; 11: 69.

5 Zhou Z, Sun S, Zou L, Schneider Y, Schmauder S, Wang M. Enhanced strength and high temperature resistance of 25Cr20Ni ODS austenitic alloy through thermos - mechanical treatment and addition of Mo. Fusion Eng. Des. 2019; 138: 175-182.

6 Park S, Lang M, Tracy CL, Zhang J, Zhang F, Trautmann C, Rodriguez MD, Kluth P, Ewing RC. Response of $Gd_2Ti_2O_7$ and $La_2Ti_2O_7$ to swift-heavy ion irradiation and annealing. ActaMater. 2015; 93: 1–11.

7 Suganya M, Ganesan K, Vijayakumar P, Gill AS, Ramaseshan R, Ganesamoorthy S. Structural, optical and mechanical properties of $Y_2Ti_2O_7$ single crystal. Scripta Mater. 2020; 187: 227 – 231.

8 Nguyen ST, Nakayama T, Suematsu H, Suzuki T, Takeda M, Niihara K. Low thermal conductivity $Y_2Ti_2O_7$ as a candidate material for thermal/environmental barrier coatings. Ceram. Int. 2016; 42(9): 11314-11323.

9 Gill JK, Pandey OP, Singh K. Ionic conductivity, structural and thermal properties of pure and Sr^{2+} doped $Y_2Ti_2O_7$ pyrochlores for SOFC. Solid State Sci. 2011; 13: 1960-1966.

10 Tao TT, Wang LX, Zhang QT. Study on the composite and properties of Y_2O_3 – TiO_2 microwave dielectric ceramics. J. Alloys Compd. 2009; 486: 606.

11 Matsushima S, Tanaka Y, Ishii J, Obata K. First-principles energy band calculation of a (Ca^{2+}, V^{5+})-doped $Y_2Ti_2O_7$ pigment. J. Ceram. Soc. Jpn. 2019; 127: 793–801.

12 Joseph D, Kaliyaperumal C, Mumoorthy S, Paramasivam T. Dependence on temperature of the electrical properties of nanocrystalline $Y_2Ti_2O_7$ ceramics. Ceram. Int. 2018; 44(5): 5426–5432.

13 Milicevic B, Marinovic-Cincovic M, Dramicanin MD. Non-isothermal crystallization kinetics of $Y_2Ti_2O_7$. Powder Technol. 2017; 310: 67–73.

14 Lee WJ, Bae DS. Synthesis and characterization of $Y_2Ti_2O_7$ photocatalytic powders by thermal assist process, in: Defect and Diffusion Forum. Trans Tech Publ. 2017; 380: 86–91.

15 Thi T, Nha N, Prakash H, Roopan M. Microwave assisted co-precipitation synthesis of MFe_2O_4 nanoferrites (M = Co and Mn) using biogenic coir extract and their physical characterization. RSC Adv. 2025; 15: 29571-29592.

16 Egorov SV, Eremeev AG, Kholoptsev VV, Rybakov KI, Sorokin AA, Balabanov SS, Rostokina EY. Enhanced densification and phase transformations during rapid microwave sintering of alumina-yttria-stabilized zirconia ceramics. J. Eur. Ceram. Soc. 2025; 45(3): 117006.

17 Zhang CT, Hu H, Cai SD, Gan FY, Cheng LC, Yao QR, Wang J. Silicon-doped yttrium titanate pyrochlore ceramics for efficient microwave absorption. J. Alloys Compd. 2026; 1062: 187616.

18 Han Q, Han J, Li Q, Gan F, Yao Q, Cheng L, Wang J. Defect engineering of Sr-doped $Y_2Ti_2O_7$ nanostructure ceramics for superior microwave absorption via air sintering. Ceramics International. In press. 2026.

19 Fernandez L, Correa D, Seguel M, Suarez C, Bustamante M, Caro C, Jana P, Leyton P, Trudel S, Cabello-Guzmán G. Catalytic photo-

degradation of brilliant green and bacterial disinfection of Escherichia coli by the action of $Y_2Ti_2O_7$/AgO films. Ceramics International. 2024; 50(14): 25241–25255.

20 Sharma R, Bisen DP, Shukla U, Sharma BG. X-ray diffraction: a powerful method of characterizing nanomaterials. Recent Research in Science and Technology. 2012; 4(8): 77-79.

21 Chen WPGZS, Chen TF, Li SL. Synthesis and Characterization of pyrochlore–type yttrium titanate nanoparticles by modified sol-gel method. Bull. Mater. Sci. 2011; 34: 429-434.

22 Li YH, Wang YQ, Zhou M, Xu CP, Valdez JA, Sickafus KE. Light ion irradiation effects on stuffed Lu2 (Ti2− xLux) O7− x/2 (x= 0, 0.4 and 0.67) structures. Nuclear Instruments and Methods in Physics Research Section B: Beam Interactions with Materials and Atoms. 2011; 269(18): 2001-2005.

23 Senthil Kumar P, Grace Pavithra K, Naushad Mu. Characterization techniques for nanomaterials, in: Nanomaterials for Solar Cell Applications. Elsevier. 2019: 97-124.

24 Mao G, Fuxia L, Qi C, Fangqiao P, Yingchen Xu, Ying Su, Lihong H. Material Science and Engineering B. 2024; 302: 117264.

25 Scimeca M, Bischetti S, Lamsira HK, Bonfiglio R, Bonanno E. Energy Dispersive X-ray (EDX) microanalysis: A powerful tool in biomedical research and diagnosis. European Journal of Histochemistry. 2018; 62(1): 2841.

26 Mahapatra A, Subudhi S, Swain S, Sahu R, Negi RR, Samanta B, Kumar P. Electrical and optical properties of yttrium titanate thin films synthesized by Sol-Gel technique. Integrated Ferroelectrics. 2019; 203(1): 43-51.

27 Li G, Yu M, Wang R, Wang Z, Quan Z, Lin J. Fabrication and photoluminescence properties of core-shell structured spherical SiO_2@ $Gd_2Ti_2O_7$: Eu^{3+} phosphors. Journal of materials research. 2006; 21(9): 2232-2240.

28 Chen ZS, Gong WP, Chen TF, Li SL. Synthesis and characterization of pyrochlore-type yttrium titanate nanoparticles by modified sol–gel method. Bulletin of Materials Science. 2011; 34(3): 429-434.

29 Akcora P, Zhang X, Kumar SK, Kofinas P. Structural and magnetic characterization of norbornene-deuterated norbornene dicarboxylic acid diblock copolymers doped with iron oxide nanoparticles. Polymer. 2005; 46(17): 7417–7424.

30 Coutier C, Meffre W, Jenouvrier P, Fick J, Audier M, Rimet R, Jacquier B, Langlet M. The Effects of Phosphorus on the Crystallisation and Photoluminescence Behaviour of Aerosol–Gel deposited SiO_2–TiO_2–Er_2O_3–P_2O_5 Thin Films. Thin Solid Films. 2001; 392(1): 40-49.

31 Subramanian MA, Aravamudan G, Subba Rao GV. Oxide Pyrochlores - A Review. Prog. Solid St. Chem. 1983; 15: 55-143.

32 Wang Z, Wang X, Zhou G, Xie J, Wang S. Highly Transparent Yttrium Titanate $Y_2Ti_2O_7$ ceramics from co-precipitated powders. Journal of Eur. Ceram. Soc. 2019; 39: 3229-3234.

33 Jasmeet KG, Pandey OP, Singh K. Ionic conductivity, structural and thermal properties of pure and Sr^{2+} doped $Y_2Ti_2O_7$ pyrochlores for SOFC. Solid State Sciences. 2011; 13(11): 1960-1966.

34 Ayman MT, Yoon DH. Review on transparent polycrystalline ceramics. J. Korean Ceramics. Society. 2022; 59: 1-24.

35 Stopikowska N, Wozny P, Suta M, Zheng T, Lis S, Runowski M. Influence of Excitation and Detection geometry on optical temperature readouts-reabsorption effects in luminescence thermometry. J. Mater. Chem. C. 2023; 11: 9620-9627.

36 Tauc J. Optical properties and electronic structure of amorphous Ge & Si. Mat. Res.Bull. 1968; 3: 37-46.

37 Pandit AK, Ansari TH, Prasad M, Singh RA, Wanklyn BM. On the electrical conductivity, thermos electric power and dielectric constant of $Y_2Ti_2O_7$ single crystals. Mats. Lett. 1991; 12: 77-83.

38 Zou Y, Ahang Y, Hu Y, Gu H. Ultraviolet detectors based on the wide band gap under nanowire: A review sensors. 2018; (18): 7.

39 Porart O, Heremans C, Tuller HL. Stability and mixed ionic electronic conduction in Gd_2 (Ti_1 – $_xMO_x)_2$ O_7 under anodic conditions. Solid State Ion. 1997; 94: 75–83.

40 Hanawa M, Maraoka Y, Tayama T, Sakakibara T, Yamawa J, Horoi Z. Super conductivity at 1 k in $Cd_2Re_2O_7$. Physics Review Letters. 2001; 87: 187001.

41 Vanheusden K, Warren WL, Seager CH, Tallant DR, Voigt JA, Gnade BE. Mechanisms behind green photoluminescence in ZnO Phosphor powders. Journal of Applied Physics. 1996; 79: 7983.

42 Tiwari H, Singh S, Kumar R, Mandal A, Pathak A, Varma NK, Kumar L, Gautam V. Novel Advancements in Nanomaterials – Based Contrast Agents Across Multimodal Imaging and Theranostic Applications. Nanoscale Advances. 2025; 7(21): 6753.

43 Nasraoui M, Bilal E, Gibert R. Fresh and weathered pyrochlore studies by Fourier transform infrared spectroscopy coupled with thermal analysis. Mineralog. Magaz. 1999; 63(4): 567-578.

44 Zhang FX, Manoun B, Saxena SK. Pressure – induced order – disorder transitions in pyrochlore $RE_2Ti_2O_7$ (RE = Y, Gd). Materials Letters. 2006; 60: 2773–6.

45 Anonymous, Pharmacopoeia of India. 3rd ed. New Delhi: Ministry of Health and Family Welfare, Government of India; 1996.

46 Taylor RSL, Manandhar NP, Hudson JB, Towers GHN. Screening of selected medicinal plants of Nepal for antimicrobial activities. Jrnl of Ethnopharmacol. 1995; 46(3): 153-159.